ENGINEERING RESEARCH JOURNAL (ERJ)

Vol. 1, No. 45 July. 2020, pp. 113 -122

Journal Homepage: http://erj.bu.edu.eg

Applied Element Method for Progressive Collapse Analysis of RC Sub-Structures

F.B.A. Beshara, O.O. El-Mahdy & M.A. Raslan

Civil Engineering Dept., Shoubra Faculty of Engineering, Benha University

Abstract. : This paper presents an applied element method-based model for the collapse analysis of reinforced concrete (RC) beam-column assemblages under middle column removal scenario. In Extreme Loading for Structures software (ELS), nonlinear constitutive material models are used for concrete and steel in joint with suitable solid and spring geometrical elements. For several validation studies, a comparison between the experimental and numerical crack patterns and failure modes is presented. All structure behavior stages till failure of specimens are simulated effectively by the presented models. This study highlights several behavior stages for beam column assemblages till the failure stage. The effect of seismic detailing, lap splice and bottom reinforcement ratio on the beam column assemblage behavior under middle column removal scenario, is also discussed and evaluated through the numerical investigation.

Keywords: Reinforced concrete; Progressive collapse; Beam-column Assemblages; Load-deflection curves; Crack patterns; Applied element method; ELS.

1. INTRODUCTION

Till 1968, structures were designed to resist ordinary loads as dead load, live load, wind and earthquake loads. While the effect of extraordinary loads such as gas explosions, fatal mistakes during construction process in addition to bomb and terrorist attacks were not well defined. In recent years, progressive collapse effects on structures attracted a significant attention by structural engineers especially after the partial collapse of Ronan point building. Then, it became an integral part of structural designing after Murrah federal building and world trade center collapse due to the terroristic attacks on them. Various definitions have been discussed the term of progressive collapse as (GSA) [1] defined the progressive collapse as “a situation where local failure of a primary structural component leads to the collapse of adjoining members which, in turn, leads to additional collapse. Hence, the total damage is disproportionate to the original cause”.

In recent years, due to increasing of terroristic attacks, the researchers developed a number of methods to analyze and design structures against the progressive collapse effect. Most of studies assured that compressive arch action and catenary action on beams are the main resisting mechanisms against progressive collapse. Beam-column assemblages testing is considered the simplified and economical method to study the resisting mechanisms against progressive collapse (Jun Yu et al. [2]; Kamal Alogla et al. [3]; Youpo Su et al. [4]; Gaurav Parmar et al. [5]; Peiqi Ren et al. [6]; Khater, A.N. [7]; Chanh Trung et al. [8]; Omid Rshidian et al. [9]; Nima Farhang Vesali et al. [10]).

In this paper, a nonlinear applied element method [11] is proposed for progressive collapse analysis of RC beam-column assemblages. Non-seismic

and seismic detailed specimens are analyzed using ELS software, and the numerical predictions are compared with the experimental results. Also, comparative study is presented for discussing the effects of seismic detailing, bottom reinforcement ratio, and lap splice on the structural response of RC beam-column sub-structures.

2. Proposed AEM for RC Sub-Structures

The applied element method (AEM) is a simple modeling and 114programming technique [12] that depends on the concept of discrete cracking. AEM predicts the highly nonlinear behavior as crack initiation, crack propagation, buckling and post-buckling behavior and progressive collapse of elements effectively with a high accuracy.

2.1 Element Discretization of Geometry

The structure in AEM is modeled as an assembly of small elements connected together along their surface by a set of normal and shear springs distributed around the element edges as shown in Figure 1 [12]. These springs represent the stresses, strains, deformations of certain area as illustrated in Figure 1 (b).

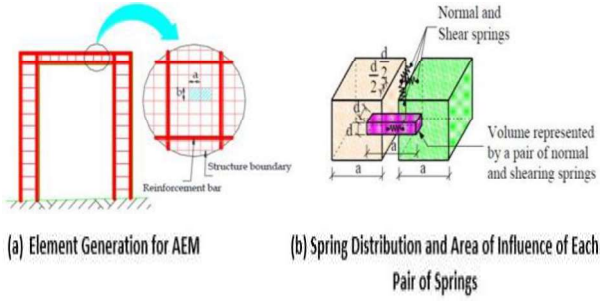

Fig 1: Modeling of Structure by AEM [12]

Each single element has six degrees of freedom; three for translations and three for rotations. Relative translational or rotational displacements between two neighboring elements cause stresses in the springs located at their common face as shown in Figure 2.

The total stiffness matrix is set by summing up the stiffness matrices of the spring around elements. The failure springs is assumed to be zero stiffness, the element stiffness matrix is determined according to the contact point location and the stiffness of normal and shear springs. The spring stiffness is calculated according to Equation 1 [12]

$$K_s = \frac{GdT}{a} \quad and \quad K_n = \frac{EdT}{a} \qquad \ldots\ldots\ldots\ldots(1)$$

Where K_s and K_n are the stiffness of shear and normal springs; d is the distance between springs; T is the thickness of the element; a is the representative area length; and E & G are the Young's and shear modulus of the material, respectively.

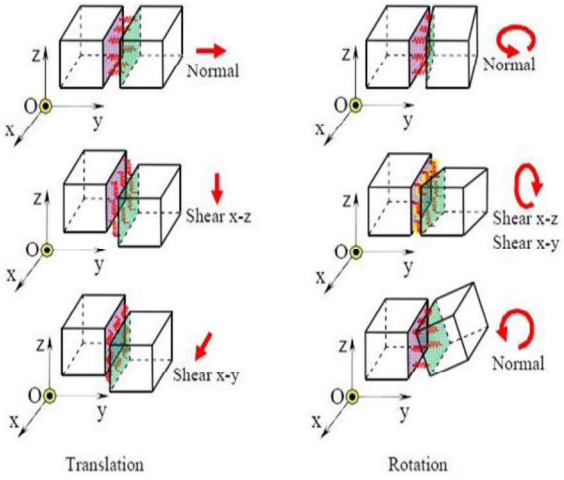

Fig 2: Stresses in springs due to Elements' Relative Displacement [13]

Each element has three degrees of freedom which represent the rigid body motion of the element, the internal stresses and deformations of it. It can be calculated by the spring deformation around each element. The element stiffness matrix can be determined by assuming that two elements which are connected only by one pair of normal and shear springs as illustrated in Figure 3. The values of dx and dy are the relative coordinate of the contact point with reference to the centroid. The degrees of freedom of the stiffness matrix are determined by assuming the unit displacement in the studied direction and the force at the centroid of each element. The element stiffness matrix size is (6x6) as shown in Figure 4 and the used notations in the stiffness matrix are mentioned in Figure 3.

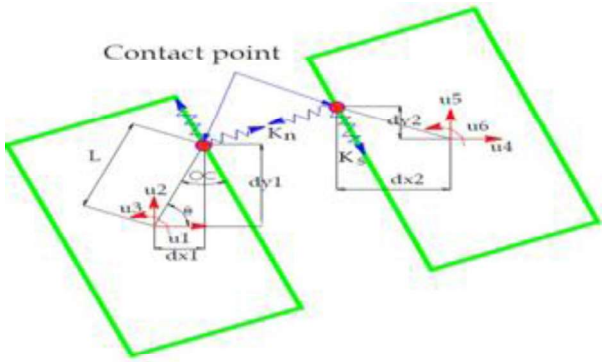

Fig 3: Element shape, contact point and DOF [12]

$$\begin{bmatrix} \sin^2(\theta+\alpha)K_n + \cos^2(\theta+\alpha)K_s & -K_n\sin(\theta+\alpha)\cos(\theta+\alpha) + K_s\sin(\theta+\alpha)\cos(\theta+\alpha) & \cos(\theta+\alpha)K_sL\sin(\alpha) - \sin(\theta+\alpha)K_nL\cos(\alpha) \\ -K_n\sin(\theta+\alpha)\cos(\theta+\alpha) + K_s\sin(\theta+\alpha)\cos(\theta+\alpha) & \sin^2(\theta+\alpha)K_s + \cos^2(\theta+\alpha)K_n & \cos(\theta+\alpha)K_nL\cos(\alpha) + \sin(\theta+\alpha)K_sL\sin(\alpha) \\ \cos(\theta+\alpha)K_sL\sin(\alpha) - \sin(\theta+\alpha)K_nL\cos(\alpha) & \cos(\theta+\alpha)K_nL\cos(\alpha) + \sin(\theta+\alpha)K_sL\sin(\alpha) & L^2\cos^2(\alpha)K_n + L^2\sin^2(\alpha)K_s \end{bmatrix}$$

Fig 4: One Quarter of Element Stiffness Matrix [12]

2.2 Constitutive Material Modeling

The main problem in using the rigid elements for modeling the reinforced concrete is the simulation of the diagonal cracks. Mohr-Coulomb's failure criteria is not valid for use in this case as it leads to increase in the resistance of the structure and inaccurate fracture behavior. Figure 5 shows the constitutive models adopted in AEM.

a) Concrete Material Model

For modeling the concrete under compression, Maekawa model [14]; shown in Figure 5(a) is used. This model introduces the initial Young's modulus, the fracture parameter, the extent of the internal damage of concrete and the compressive plastic strain to identify the envelope for compressive stresses and strains. Spring stiffness is assumed to be 1% of the initial value to avoid negative stiffness after peak stresses. Which results differences between the calculated stress and stresses from spring strain. This difference is redistributed by applying the redistributed force values in the reverse direction of the next loading step.

Spring stiffness is assumed as the initial stiffness until reaching the cracking point for the concrete springs subjected to tension, these springs is set to be zero after cracking. The relationship between shear stress and shear strain as illustrated in Figure 5(a) is assumed to be linear till the concrete cracking, and then the shear stresses drop down due to the aggregate interlock and friction at the crack surface.

b) Steel Material Model

The model introduced by Ristic et al. [15] is used for modeling reinforcement springs as shown in Figure 5(b). The tangent stiffness of reinforcement is calculated according to the strain from the reinforcement spring, loading status and the previous history of steel spring which controls the Bauschinger's effect. This model can consider easily the effect of partial unloading and Bauschinger's effect. The reinforcement bar is assumed to be cut after reaching 10% of its tensile strain and the force carried by the reinforcement bar is redistributed.

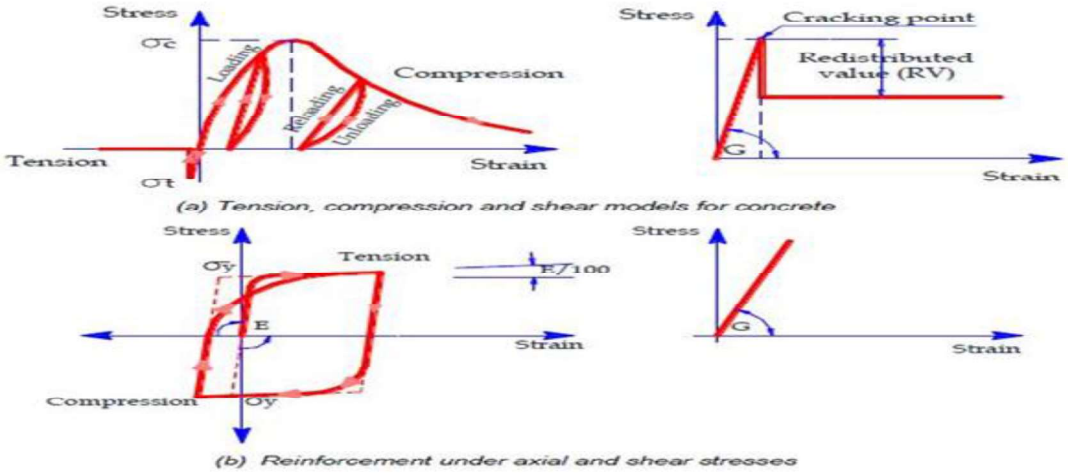

Fig 5: Constitutive Models for Concrete and Steel [14], [15]

3. Validation Studies for Non-Seismic Detailed Specimens

Two experimental beam column assemblages with non-seismic detailing conducted by Yu et al. [2] are selected and modeled using ELS software. Each sample has two equal spans; the interior column was removed to consider the effect of progressive collapse.

3.1 Model Description of Selected Specimens

Two beam column assemblages with the same dimensions were selected and labeled as S2 and S4 [2]. The beams dimensions are 150 mm in width, 250 mm in depth with cover 20 mm and span of 2750 mm. The exterior columns cross section dimensions are 450 x 400 mm, while the middle column dimensions are 250 x 250 mm. The steel reinforcement for the two specimens were different, as the top and bottom reinforcement ratio for S2 at the middle section was 0.49% while at the beam ends was 0.73% for the top reinforcement and 0.49% for the bottom reinforcement. For specimen S4, the top and bottom reinforcement ratio at the middle section was 0.82%. However, at the beam ends was 1.24% for top reinforcement and 0.82% for bottom reinforcement. The reinforcement details and concrete dimensions for the specimens are shown in Figure 6, while the material properties are mentioned in Table 1. One of the main reinforcement detailing differences between the two samples is the existence of a lap splice at the bottom bars at middle joint for specimen S2, while the bottom reinforcement bars at middle joint for S4 are continuous without any splices.

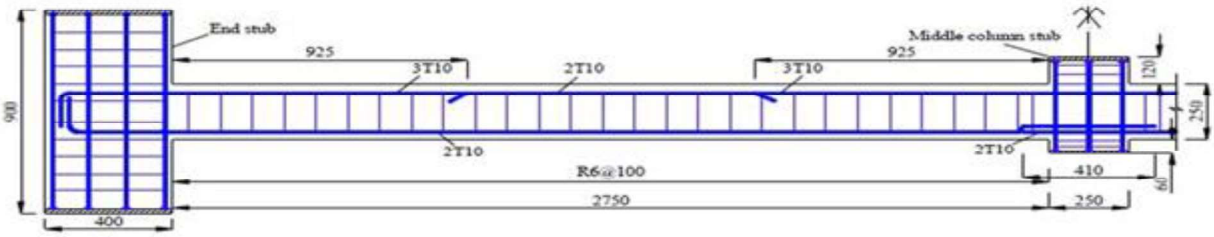

a) Specimen S2 Details [2]

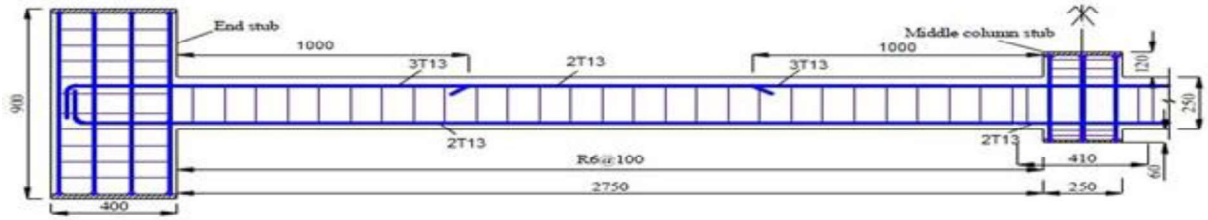

b) Specimen S4 Details [2]

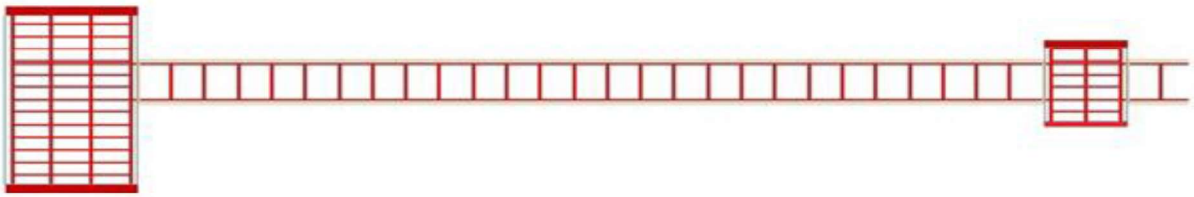

c) ELS Model Reinforcement Details

Fig 6: Specimens Details and Modeling

Table 1: Specimens Material Properties [2]

i) Concrete

Young's Modulus	Tensile Stress	Compressive Stress	Rupture Strain
(GPa)	(MPa)		
29.6	3.5	38.2	**0.2**

ii) Reinforcement

Bar Diameter	Yield Stress	Ultimate Stress	Rupture Strain
(mm)	(MPa)		
R6	349	459	**0.15**
T10	511	622	**0.21**
T13	494	593	**0.21**

For the two specimens, 3D models were performed to simulate the experimental works conducted by Yu et al. [2]. The load was applied under displacement control, the top and bottom of two end column were restrained from horizontal movement by a two roller support. In these two models, all reinforcement details have been taken into consideration. The loading process is applied into two stages; in the first stage the own weight of the structural elements is applied statically. The middle column is removed in the second stage and replaced by adding a static displacement load of 650 mm over 1300 loading increments.

3.2 Predicted Load-Deflection Curves

Figure 7 shows the load-deflection curves at middle column location for the predicted numerical and experimental results. Also, the results of the two beam column assemblages are mentioned in Table 2. It is clear that there is a considerable agreement between the numerical and the experimental results.

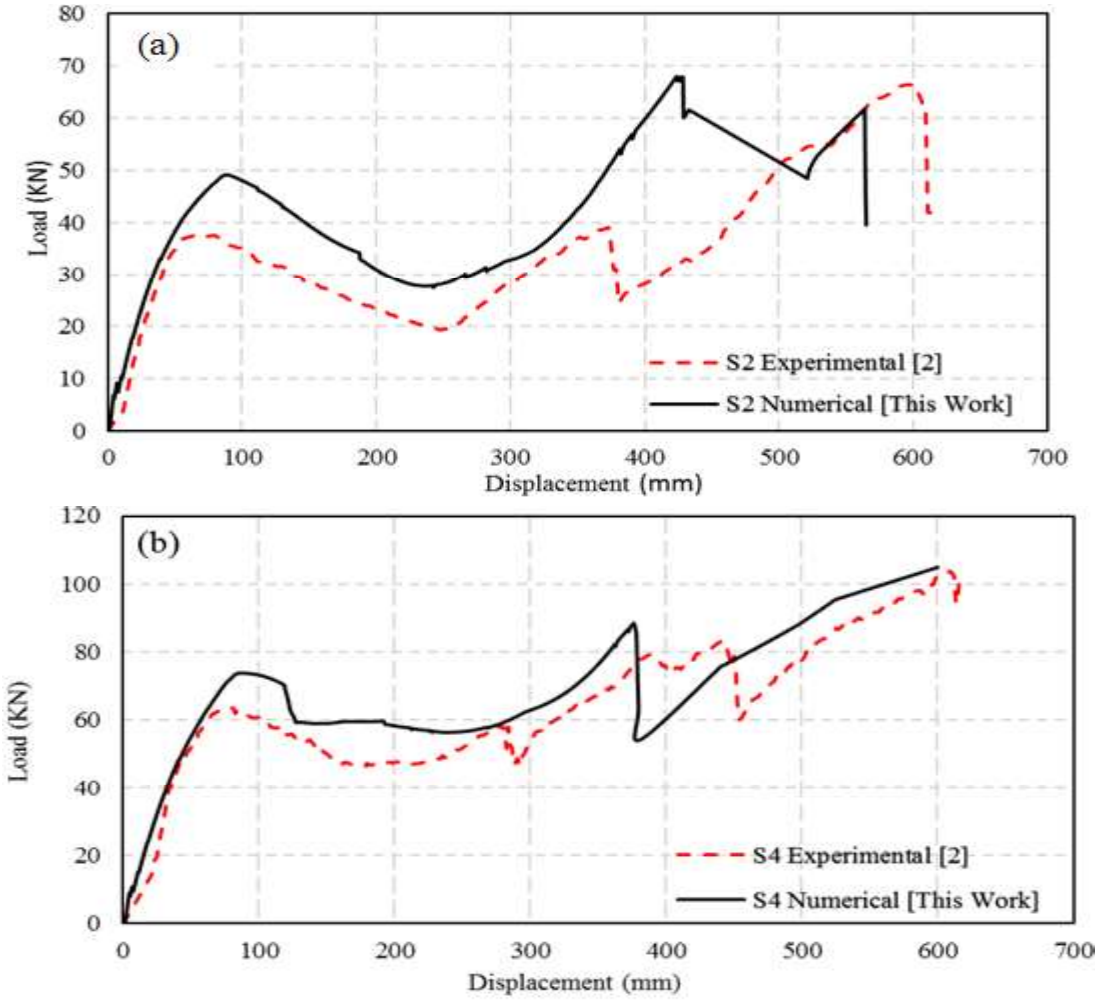

Fig 7: Experimental and Numerical Load - Deflection Curves

The three progressive collapse resisting mechanisms; flexural action, compressive arch action (CAA) and catenary action (CA) have been occurred for the two specimens. As shown in Figure 7(a), plastic hinges for specimen S2 have been created after the yielding of the top and bottom reinforcement at load of 34.33 kN in the numerical model, and of 29.02 kN in the experimental test which is considered as a good estimation for the experimental result, then it reached the peak load level at a displacement ratio between the two results equal 0.86 with a very small difference. The specimen failed when the predicted numerical displacement reached 562.29, which is lower than the experimental result (612 mm) by only 10%.

Figure 7(b) shows the experimental and numerical results for specimen S4. At the beginning of loading, the two curves were perfectly close and the first cracking load ratio between the two curves were 0.92, which is a very good estimation to this stage results. When reaching the CAA point, small differences in the load values have been noticed with considerable prediction for the displacement of this stage. At the failure stage, the differences between the two points of the catenary point were only 2% for the load and displacement, which proves that the proposed model gives a realistic prediction for the progressive collapse scenarios and effects.

Table.2: Experimental Results in Comparison to Numerical Results

Specimen	Experimental Results [2]			Numerical Results [This work]			Experimental/Numerical		
	(kN)								
	P^E_f	P^E_{CAA}	P^E_{CA}	P^N_f	P^N_{CAA}	P^N_{CA}	P^E_f / P^N_f	P^E_{CAA} / P^N_{CAA}	P^E_{CA} / P^N_{CA}
S2	29.02	38.38	67.63	34.33	48.98	61.43	0.85	0.78	1.10
S4	47.76	63.22	103.68	51.83	88.56	105.2	0.92	0.71	0.98
Specimen	(mm)								
	Y^E_f	Y^E_{CAA}	Y^E_{CA}	Y^N_f	Y^N_{CAA}	Y^N_{CA}	Y^E_f / Y^N_f	Y^E_{CAA} / Y^N_{CAA}	Y^E_{CA} / Y^N_{CA}
S2	22.17	73	612	30.1	85.38	562.29	0.74	0.86	1.10
S4	43.1	81	614.3	44.8	73.95	601.3	0.96	1.10	1.02

where P_f: Flexural Load, P_{CAA}: Peak Load, P_{CA}: Catenary Load, Y_f: Flexural Displacement, Y_{CAA}: Peak Displacement, Y_{CA}: Catenary Displacement

3.3 Predicted Failure Mode and Cracking Patterns

A comparison between the failure and cracks modes between the ELS model and the experimental test at the middle and end joint for the two samples are shown in Figure 8. The figure shows a good agreement between the numerical model and the experimental cracking patterns. The figure presents the fracture of bars at the middle joint which is simulated perfectly on ELS. The middle joint of the two specimens is failed before the top bars fracture at the end joints. A concentration of cracks at the interface between the beam and middle column for specimen S4 which has a continuous bottom reinforcement. While, two wide cracks are generated at the free ends of spliced bars at specimen S2.

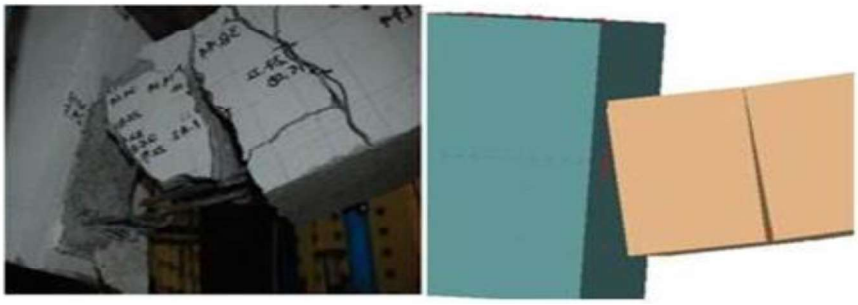

a) Middle Joint Fracture of Specimen S2

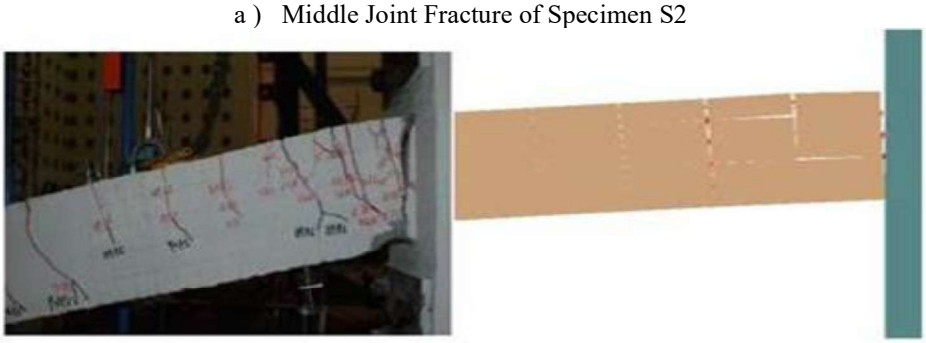

b) End Joint Fracture of Specimen S2

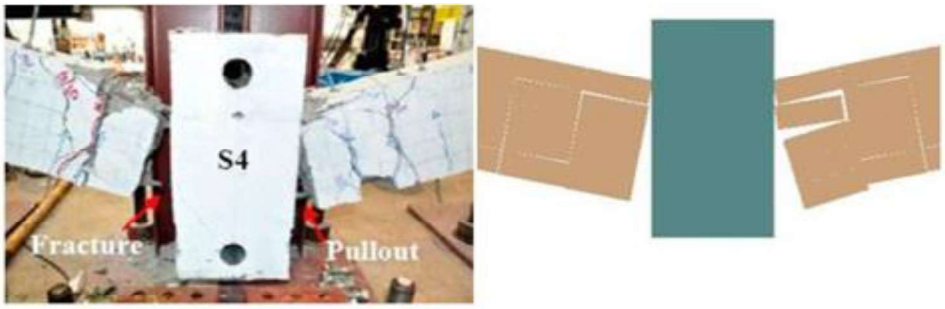

c) Middle Joint Fracture of Specimen S4

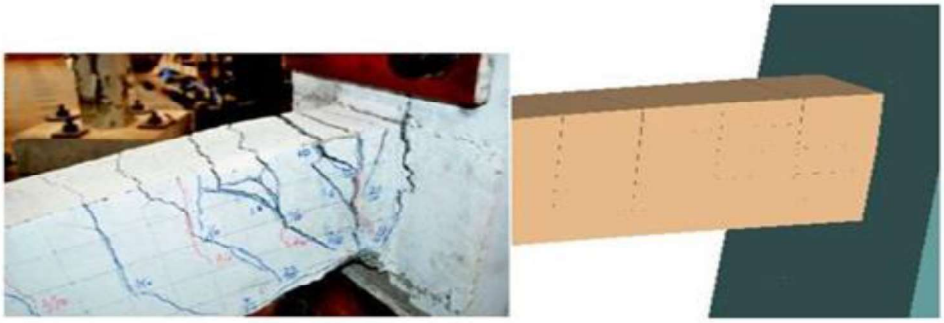

d) End Joint Fracture of Specimen S4

Fig 8: Crack Patterns for Specimens S2 and S4

4.Validation Studies for Seismic Detailed Specimens

4.1 Model Description of Selected Specimen

A seismic detailed beam column assemblage presented by Yu et al. [2] is simulated using ELS software. Specimen S1 is having the same beams and columns dimensions as the non-seismic detailed ones. The longitudinal reinforcement ratio at the end section is 0.9% for the top bars and 0.49% for the bottom bars. For the middle section, the reinforcement ratio for the top and bottom bars equal 0.49%. The reinforcement details and concrete dimensions are shown in Figure 9, while the material properties are shown in Table 1. A static displacement load of 650 mm is applied over 1300 loading increments.

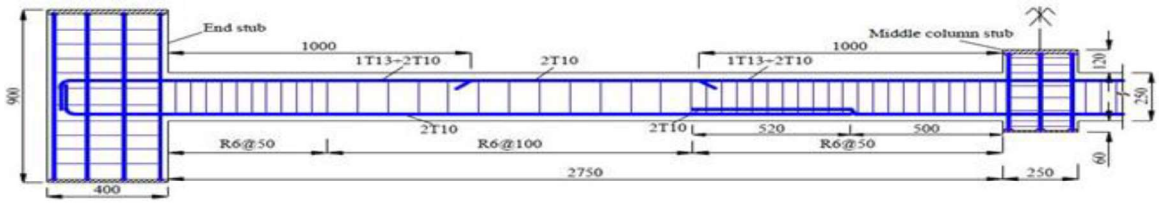

a) Specimen S1 Details [2]

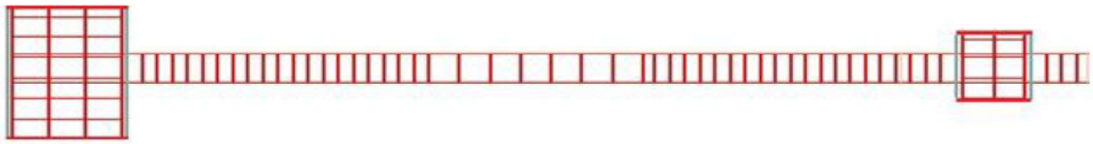

b) ELS Model Reinforcement Details

Fig 9: Specimen S1 Details and Modeling

4.2 Predicted Load-Deflection Curve at Middle Joint

As shown in Figure 10 and Table 3, there is a good agreement between the experimental and numerical results. The plastic hinge for S1 occurred after bottom reinforcement yielding at 53.85 mm for the numerical model, and then it reached its peak load at 52.53 kN with a 0.87 ratio to the experimental result. The specimen failed when reaching displacement of 616.45 kN with only 0.07 % difference from the experimental result

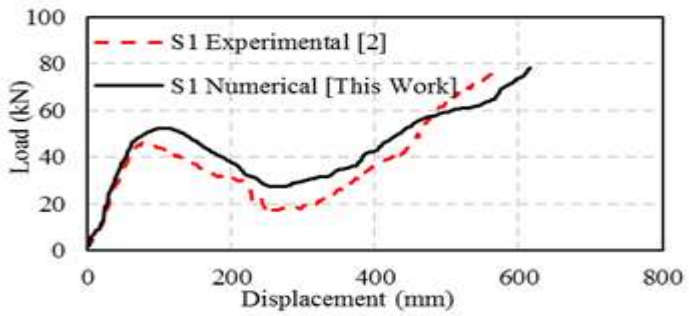

Fig 10: Experimental and Numerical in Load Deflection Curves Results

Table 3: Experimental Results Comparison to Numerical Results

		Exp.	Num.	Exp./Num.
P_f	kN	36.39	41.51	0.88
P_{CAA}		45.8	52.53	0.87
P_{CA}		81.74	88.73	0.92
Y_f	mm	46.41	53.85	0.86
Y_{CAA}		78	107.69	0.72
Y_{CA}		573	616.45	0.93

4.3 Predicted Failure Mode and Cracking Patterns

By comparing the numerical and experimental crack patterns at the middle and end joints, there is a considerable similarity between the failure modes of AEM and the laboratory test. The cracks are concentrated on the column face at the point of intersection between the beam and column at middle and end joints.

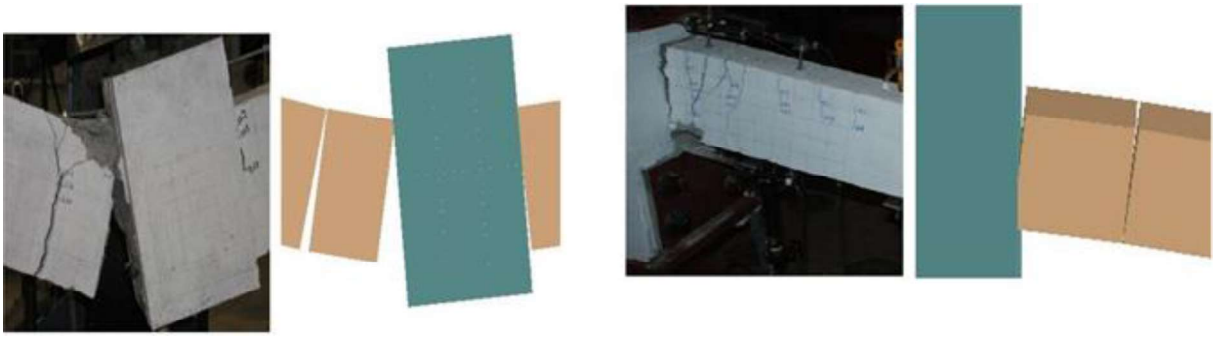

Fig 11: Observed and Predicted Crack patterns for Specimens S1

5. Overall Evaluation of Modeled Specimens

A comparison between the results of the three specimens is shown in Figure 12. The following points represent the observations noticed on their results:

1) Specimens S1 and S2 represent the difference between the seismic and non-Seismic detailing effect. The two curves are almost similar until reaching the compressive arch action point. The seismic detailing increases the load at failure by 12% and the displacement by 10%. Also, there a significant residual strength in the catenary action ranges.
2) For different response stages, the increase in the bottom reinforcement ratio for specimen S4 resulted in an increase of the resistance of the assemblage to the progressive collapse with a slight difference in the displacement results. As well as, the lap splice of bottom steel of specimen S2 caused a wide crack at the free end of the spliced bars.

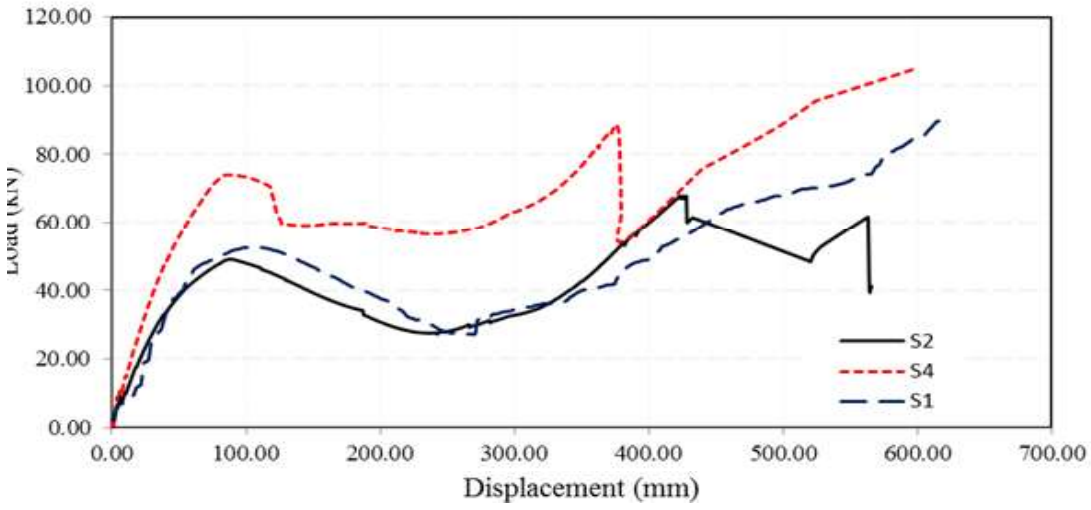

Fig 12: Numerical Load - Deflection Curves for All Specimens

Conclusions

In this paper, an applied element model is proposed using ELS software. From the modeling and validation study with the experimental works conducted by Yu et al. [2], the following main conclusions are drawn:

1. The proposed nonlinear applied element technique is proofed that it is an effective method to predict the behavior of the progressive collapse beam column assemblage under middle column removal scenario. For different types of assemblages, there is a good agreement between the numerical predictions and the experimental results.

2. ELS software presents a good numerical tool to predict the entire load-deflection curves, crack patterns and failure modes; compared to the experimental shape of cracks. The elastic stage, CAA stage and catenary stage are well-predicted and estimated in the conducted numerical models till final failure of RC sub-structures.

3. Compared with the non-seismic detailed specimen, the seismic detailed assemblage has a higher strength and stiffness. At the compressive arch action point, the load and corresponding displacement are increased by 10% and 12%, respectively. Also, there a significant residual strength in the catenary action ranges.

4. For different response stages, the increase in the bottom reinforcement ratio for specimen S4 resulted in an increase of the resistance of the assemblage to the progressive collapse with a slight difference in the displacement results. As well as, the use of continuous bottom reinforcement without lapped splices causes narrow and distributed cracks at beam-column assemblages.

REFERENCES

[1] General Services Administration (GSA), "Alternate Path Analysis and Design Guidelines for Progressive Collapse Resistance", (2013), Washington DC: General Services Administration.

[2] Yu,J. and Tan, K. H.," Structural Behavior of RC Beam-Column Sub assemblages under a Middle Column Removal Scenario," Journal of Structural Engineering, Vol.139, No. 2, Feb. (2013), pp. 233-250.

[3] Alogla, K., Weekes, L., and Nelson, L.A., "Progressive Collapse Resisting Mechanisms of Reinforced Concrete Structures", Proceedings of the 5th International Conference on Integrity-Reliability-Failure, Porto/Portugal, 24-28 Jul. (2016).

[4] Su, Y., P., Tian, Y. and Song, X. S., “Progressive Collapse Resistance of Axially-Restrained Frame Beams.” ACI Structural Journal, Vol. 106 (5), (2009), pp. 600-607.

[5] Parmar, G., Joshi, D.D., and Patel, P.V.," Experimental Investigation of RC Beam-Column Assemblies under Column Removal Scenario", Nirma University Journal of Engineering and Technology (NUJET), Vol. 3, No. 1, (2015), pp. 15-20.

[6] Ren, P., Li, Y., Lu, X., Guan, H., and Zhou, Y., "Experimental Investigation of Progressive Collapse Resistance of One-Way Reinforced Concrete Beam–Slab Substructures under a Middle-Column-Removal Scenario", Engineering Structures, Vol. 118, (2016), pp. 28-40.

[7] Khater, A.N., "Progressive Collapse Assessment of Reinforced Concrete Beam-Column Assemblages", Ph.D. Thesis, Benha University, Shobra Faculty of Engineering, Egypt, (2020).

[8] Chanh, T.H., Jongyul, P., Jinkoo, K., "Progressive Collapse-Resisting Capacity of RC Beam–Column Sub-Assemblage, "Magazine of Concrete Research Vol.63, No.4, (2011), pp. 297-310.

[9] Rashidian, O., Abbasnia, R., Ahmad, R., and Nav, F.M., "Progressive Collapse of Exterior Reinforced Concrete Beam–Column Sub-Assemblages: Considering The Effects of a Transverse Frame", International Journal of Concrete Structures and Materials, Vol. 10, No.4, Dec. (2016), pp. 479–497.

[10] Vesali, N.F., Valipour, H., Samali, B., and Foster, S., "Development of Arching Action in Longitudinally-Restrained Reinforced Concrete Beams", Construction and Building Materials, Vol. 47, (2013), pp. 7-19.

[11] Raslan, M.A., "Approaches for Resisting Progressive Collapse in Reinforced Concrete Buildings", M.Sc. thesis to be submitted, Benha University, Shobra Faculty of Engineering, Egypt, (2020).

[12] Meguro, K. and Tagel-Din, H, "Applied Element Method for Structural Analysis: Theory and Application for Linear Materials", Structural Eng. /Earthquake Eng., International Journal of the Japan Society of Civil Engineers (JSCE), (2000) 17, 21s-35s.

[13] Applied Science International, "Extreme Loading for Structures", Theoretical Manual, Durham, NC, (2013), (General).

[14] Okamura, H. and K. Maekawa, "Nonlinear Analysis and Constitutive Models of Reinforced Concrete", Gihodo Co. Ltd., Tokyo, (1991).

[15] Ristic, D., Yamada, Y., and Iemura, H., "Stress-Strain Based Modeling of Hysteretic Structures under Earthquake Induced Bending and Varying Axial Loads", (1986), Research report No. 86-ST-01, School of Civil Engineering, Kyoto University, Kyoto, Japan.